




Analysis and design of weak coupling coupler based on the half mode substrate integrated waveguide

Minghui You , Guohua Liu and Zhiquan Cheng

School of Electronic and Information Engineering, Hangzhou Dianzi University, Hangzhou, 310018, China

Research Paper

Cite this article: You M, Liu G, Cheng Z (2023). Analysis and design of weak coupling coupler based on the half mode substrate integrated waveguide. *International Journal of Microwave and Wireless Technologies* **15**,734–741. <https://doi.org/10.1017/S1759078723000156>

Received: 4 November 2022

Revised: 19 February 2023

Accepted: 21 February 2023

Keywords:

Substrate integrated waveguide, Weak coupling coupler, Even-odd mode, Ku-band

Author for correspondence:

Guohua Liu, E-mail: ghliu@hdu.edu.cn

Abstract

Substrate integrated waveguide (SIW) technology represents a good solution for the design of couplers. Coupler structures proposed in most relevant reports cannot achieve excellent performance in the case of weak coupling. This work proposes a new weak coupling coupler architecture, similar to the branch line coupler. The metal via arrays is used to reshape the electric field distribution of the SIW structure, making the overall structure achieve weak coupling characteristics. The even-odd mode decomposition method analyzes this structure's equivalent transmission line model. For this purpose, a systematic design procedure is deployed to achieve several coupling values over a wide frequency bandwidth. A novel half-mode substrate integrated waveguide (HMSIW) coupler with a 29 dB coupling is designed and fabricated for verification based on the proposed method. Good agreements between the calculated and simulated results are observed. The proposed coupler has the advantage of high directivity within the broadband and can be used for SIW-based circuits and power detection in the Ku-band.

Introduction

The past twenty years have seen increasingly rapid advances in substrate integration technology [1], and the substrate integrated waveguide (SIW) has been extensively used for wireless communication systems. The SIW can seamlessly integrate with other transmission lines because of its unique structure. This technique not only has the characteristics of high Q factor and low insertion loss like the metal waveguide but also has the advantages of a compact profile, low cost, and easy fabrication of microstrip lines [2]. Microwave and Millimeter-wave devices based on the SIW techniques are emerging in an endless stream, and a large number of papers on passive devices such as couplers, filters, power dividers, and antennas, as well as active devices such as power amplifiers [3–9]. Previous research has established that SIW structures can serve as a good solution for coupler design. In [10], a novel component of the half-mode substrate integrated waveguide (HMSIW) 3 dB coupler is proposed. This structure achieves a nearly 50% reduction in size without deteriorating the performance of the SIW. Reference [11] proves the feasibility of H-plane multi-aperture SIW couplers. In 2020, [12] proposes the HMSIW directional coupler with high common-mode suppression. In [13], a 20 dB SIW coupler operating at 36~42 GHz with four holes opened on the narrow wall is designed to achieve weak coupling for the 5G communication system applications. However, most studies on SIW couplers have only focused on 3 dB couplers. These coupler structures proposed in most relevant reports can't achieve excellent performance in the case of weak coupling.

So far, most of the methods mentioned in the literature to study the coupling characteristics of SIW couplers are too cumbersome, which greatly reduces the design efficiency of SIW couplers. In [14], Zheng Liu adopts a simplified ray tracing method to approximate and predicts the coupling characteristics of an H-plane multi-aperture SIW coupler. The paper provides a simple and effective way to determine the geometric parameters of the multi-aperture coupler based on the SIW. In 2020, Xiyao Wang proposes an equivalent transmission line model to analyze the coupling of SIW couplers [15], providing a simple and accurate method to estimate the coupling between two closely spaced SIWs sharing a row of metal cylinders simplifying the design method of SIW couplers. The conventional coupler structure based on SIW is too simple, designers lack design variables to effectively control the coupling coefficient, which has become one of the bottlenecks of SIW coupler design.

This paper presents a new broadband HMSIW coupler suitable for weak coupling mode. The main contribution and novelty of this work is the introduction of a branch-line like coupling structure. The equivalent transmission line models of the SIW coupling structures are extracted and analyzed using the even-odd mode decomposition method. This structure brings new design variables, so designers can more effectively control the coupling coefficient of the

SIW structure. Furthermore, the analysis and complete design procedure are provided, where a novel weak coupling SIW coupler is proposed and fabricated. The designed coupler has the advantages of broadband, high flatness in the band, good directivity, and ease of manufacture, which can be applied to design SIW-based circuits and power sensing in the Ku-band.

The remaining part of the paper proceeds as follows. The proposed coupling characteristics analysis of SIW structures and design procedure are presented in the second part. The third part compares and analyzes the simulation and measurement results of the proposed HMSIW weak coupling coupler. Finally, a conclusion is given in the fourth part.

The analysis of design theory

The traditional SIW is integrated on the dielectric laminate, which is arranged by two lines of conducting metallic vias with the same size and spacing. This structure significantly reduces the radiation losses caused by the leakage through the gaps between vias on the dielectric. The SIW is equivalent to a conventional metallic waveguide, and different forms can only transmit a single TE or TM mode. Although the volume of the SIW is much smaller than the waveguide, the plane size is still considerable. The HMSIW is only half of SIW [10]. The vertical center plane along the direction of propagation is an electric field maximum when the SIW operates in the main mode, so this center plane can be considered an equivalent magnetic wall. With this virtual magnetic wall, the SIW can be divided into two parts, and each half of the SIW becomes an HMSIW structure. The cost of size reduction is that there will be an inevitable radiation loss along the open boundary [16]. The operating frequency of the directional coupler should be higher than the cutoff frequency of HMSIW to ensure good transmission performance of the device. In addition, the operating mode of HMSIW should be set to mode TE₁₀. The design formula of cutoff frequency f_{mn} and the geometric parameters of the SIW resonator are given by [17]

$$f_{mn} = \frac{c}{2\pi\sqrt{\epsilon_r\mu_r}} \sqrt{\left(\frac{m\pi}{W_{eff}}\right)^2 + \left(\frac{n\pi}{L_{eff}}\right)^2} \tag{1}$$

$$W_{eff} = W - \frac{d^2}{0.95p} \tag{2}$$

$$L_{eff} = L - \frac{d^2}{0.95p} \tag{3}$$

$$W_H = \frac{W_{eff}}{2} \tag{4}$$

$$\frac{p}{d} < 2.5 \tag{5}$$

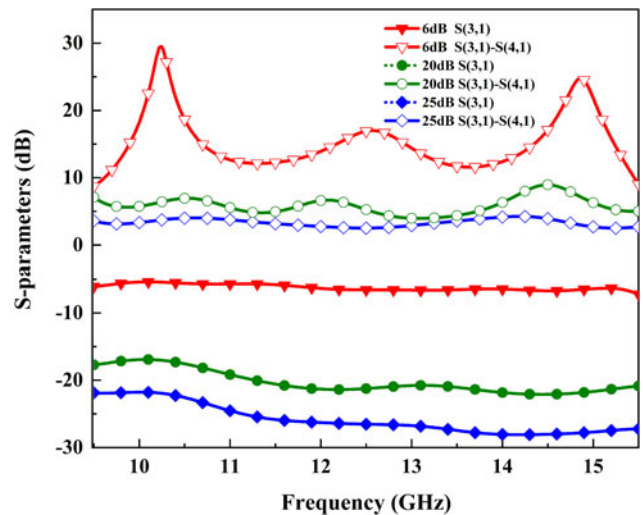


Fig. 2. Comparison of coupling and directivity under different lengths of coupling gaps.

where W_{eff} and L_{eff} denotes the effective width and length of the SIW cavity; c is the velocity of light in the free space; μ_r is the relative permeability of the substrate, and ϵ_r is the relative permittivity of the substrate. Equation (4) indicates that the HMSIW equivalent width W_H is half the SIW. The parameters of metal vias affect the radiation boundary of HMSIW. The following condition has been considered by equation (5) to eliminate radiation loss. Here, p stands for the gap between metal vias, and d is the diameter of the metal vias.

The geometrical configuration of the HMSIW forward-directional coupler is shown in Fig. 1. It consists of two HMSIW sharing a row of metal via walls, with a coupling gap in the middle for coupling. SIW-microstrip transition is necessary to facilitate the measurement of material objects and integration with other transmission lines. It is worth noting that it will bring some insertion loss. The length of the coupling gap W_{gap} in Fig. 1 determines the coupling. Port 1 is the input port, Port 2 is used as the through port, Port 3 is the coupling port, and Port 4 is named the isolation port.

Figure 2 shows the coupling and directivity of the HMSIW coupler under different coupling gap widths. It can be seen that such a structure can get good performance in the intense coupling mode, and the directivity can reach more than 12 dB. In addition, the directivity deteriorates when controlling the coupling gap W_{gap} to implement a weak coupling mode such as 20 and 25 dB, and the flatness of the weak coupling is worse than the strong coupling. Achieving high directivity and excellent flatness in the weak coupling mode is challenging.

The SIW couplers with different coupling structures are proposed in [10–15, 18–20]. However, the biggest problem with



Fig. 1. Schematic of half mode substrate integrated waveguide coupler.

these coupling structures is that the design variables are single, and the coupling coefficient cannot be effectively controlled. This paper introduces several controllable design variables by adding the metal via arrays. First, we must discuss the transmission line discontinuity caused by adding metal via arrays. As shown in Fig. 3(a), a pair of metal vias perpendicular to the signal transmission direction is added to the HMSIW structure, and the length of the metal vias is W_{ve} . Figure 3(b) shows the equivalent circuit diagram of the waveguide structure. The introduction of metal via row can be equivalent to a parallel LC resonant circuit. For HMSIW symmetrical structure, the odd mode impedance and even mode impedance of the whole coupling structure can be calculated

$$Z_{0e1} = Z_{0e} \left(1 + jZ_0 \left(-\frac{1}{\omega C_1} + \omega L_1 \right) \right)^{-1} \quad (6)$$

$$Z_{0o1} = Z_{0o} \left(1 + jZ_0 \left(-\frac{1}{\omega C_1} + \omega L_1 \right) \right)^{-1} \quad (7)$$

where Z_{0e1} and Z_{0o1} represent the coupling transmission line's even-mode and odd-mode impedance after adding the vertical walls, respectively. Z_{0e} , Z_{0o} , and Z_0 represent the coupling transmission line itself as the even-mode impedance, odd-mode impedance, and characteristic impedance, respectively. L_1 and C_1 are inductance and capacitance of the LC parallel circuit. It

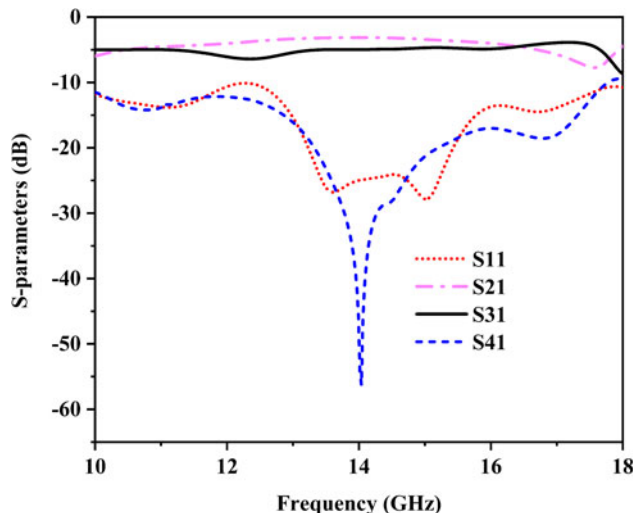
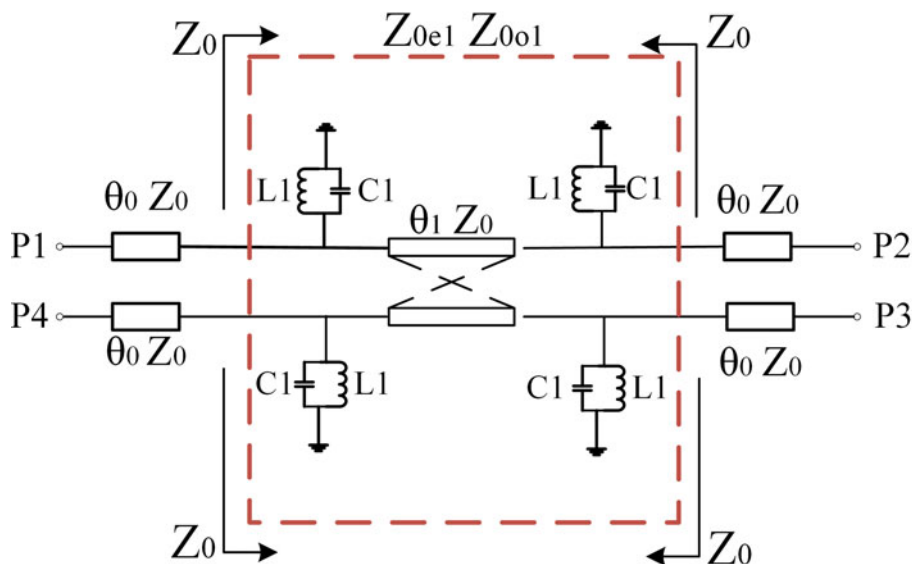


Fig. 4. Simulated S-parameters of the vertical metal walls loaded HMSIW coupler.

can be seen that the addition of metal vias will only introduce the imaginary part value without additional loss. To test the theory, Fig. 4 shows the S parameters of the HMSIW coupler after adding metal via walls. The insertion loss S_{21} and coupling coefficient S_{31} have not changed. Due to the resonance characteristics of the LC circuit, S_{41} of the whole coupler has been dramatically



(a)



(b)

Fig. 3. Schematic of (a) vertical metal walls loaded HMSIW coupling structure and (b) the equivalent circuit modal.

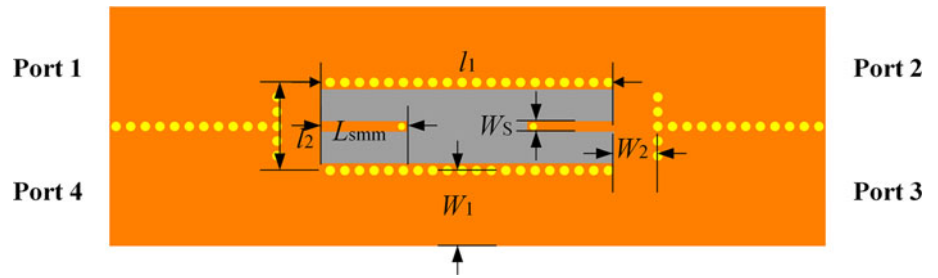


Fig. 5. Schematic diagram of the weak coupling coupler with compensation structure.

improved at the central frequency point, but the bandwidth has been reduced. In a word, the reasonable introduction of metal via arrays will not bring more losses and can be used in the design of SIW couplers.

Figure 5 depicts the HMSIW coupling topology proposed in this paper. The overall architecture is similar to the branch line coupler. It is divided into three transmission lines with different characteristic impedances and equivalent lengths, used as the feeder, direct branch, and coupling branch, respectively. This way, multiple controllable variables are introduced to control the coupling coefficient. In addition, a compensation structure based on the symmetrical parallel short stubs is added to the central hollowed area. The structure introduces the reactance value into the coupling branch. The directivity and coupling of

the whole band can be optimized by changing the compensation structure's size to improve the performance of the coupler.

The equivalent circuit model of the HMSIW weak coupling coupler is shown in Fig. 6(a). In order to deduce the detailed design process, the odd and even mode equivalent circuit is carried out for the four-port coupling network composed of the straight branch and coupling branch, as shown in Figs 6(b) and 6(c). Although mining a portion of the metal layer will result in loss G , the focus of this discussion is not on insertion loss, which can be omitted from the derivation of the formulas. B is the equivalent capacitance of the compensation structure.

According to the transmission line and matrix theory, the ABCD matrix A_e of the two-port even-mode equivalent circuit

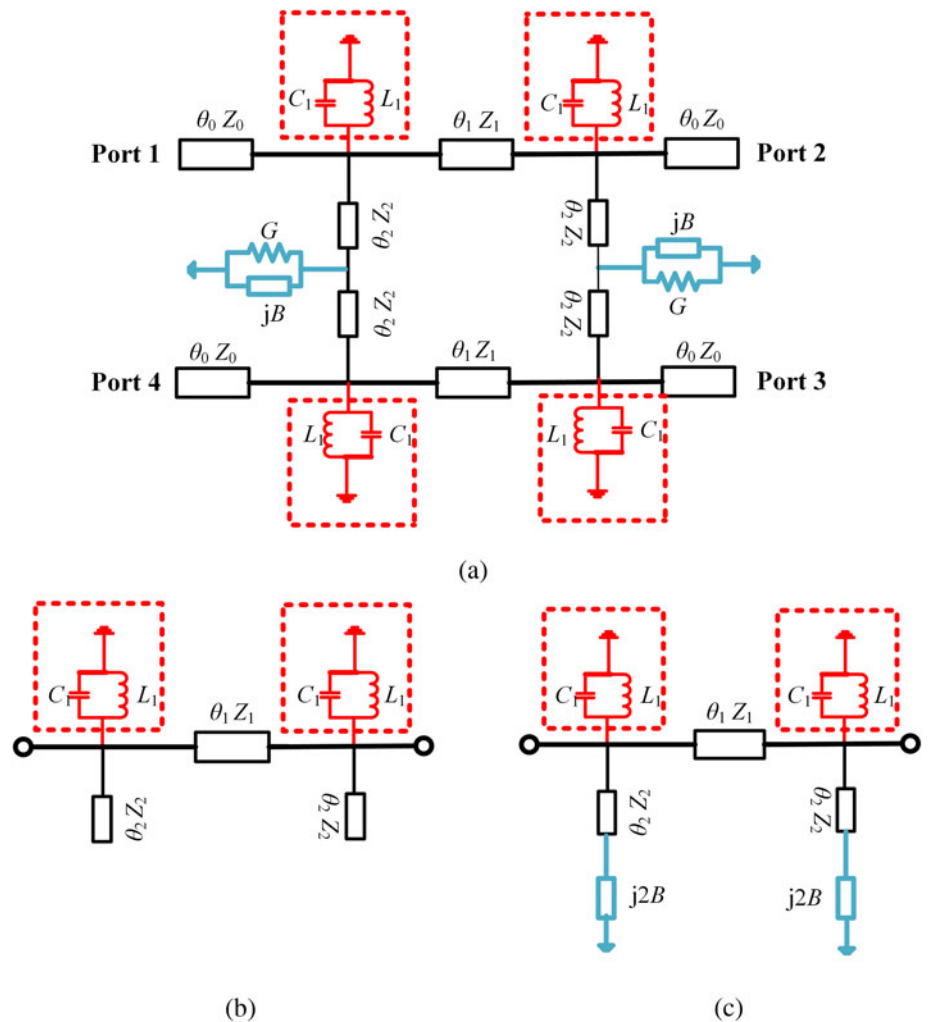


Fig. 6. (a) Topology of overall equivalent circuit, (b) odd-mode, and (c) even-mode equivalent circuit of the proposed novel weak coupling coupler.

can be expressed as

$$A_e = \begin{pmatrix} a_{11e} & b_{12e} \\ c_{21e} & d_{22e} \end{pmatrix} = \begin{pmatrix} \cos \theta_1 - Z_1 \sin \theta_1 T_e & jZ_1 \sin \theta_1 \\ j\cos \theta_1 T_e + \frac{j \sin \theta_1}{Z_1} & -Z_1 \sin \theta_1 T_e + \cos \theta_1 \\ +jT_e(-Z_1 \sin \theta_1 T_e + \cos \theta_1) & \end{pmatrix} \quad (8)$$

where

$$T_e = \omega C_1 + \frac{1}{\omega L_1} + 2B + \frac{\sin \theta_1}{Z_2} \quad (9)$$

The S-parameter of the even-mode equivalent circuit can then be derived as

$$S_{11e} = \frac{j(Z_1 \sin \theta_1 - 2\cos \theta_1 T_e - (\sin \theta_1 / Z_1) + Z_1 \sin \theta_1 T_e^2)}{\Psi_e} \quad (10)$$

$$S_{21e} = \frac{2}{\Psi_e} \quad (11)$$

where

$$\Psi_e = 2(\cos \theta_1 - Z_1 \sin \theta_1 T_e) + j\left(2\cos \theta_1 T_e + Z_1 \sin \theta_1 + \frac{\sin \theta_1}{Z_1} - T_e^2 Z_1 \sin \theta_1\right) \quad (12)$$

Similarly, the S-parameter of an odd-mode equivalent two-port circuit can be obtained

$$S_{11o} = \frac{j(Z_1 \sin \theta_1 - 2\cos \theta_1 T_o - (\sin \theta_1 / Z_1) + Z_1 \sin \theta_1 T_o^2)}{\Psi_o} \quad (13)$$

$$S_{21o} = \frac{2}{\Psi_o} \quad (14)$$

where

$$T_o = \omega C_1 + \frac{1}{\omega L_1} - \frac{\sin \theta_1}{Z_2} \quad (15)$$

$$\Psi_o = 2(\cos \theta_1 - Z_1 \sin \theta_1 T_o) + j\left(2\cos \theta_1 T_o + Z_1 \sin \theta_1 + \frac{\sin \theta_1}{Z_1} - T_o^2 Z_1 \sin \theta_1\right) \quad (16)$$

The characteristic impedance Z_i of the HMSIW transmission lines can be expressed as

$$Z_i = R_i + jX_i (i = 0, 1, 2) \quad (17)$$

For the lossless case, $R_i = 0$, and hence

$$X_i = \frac{60\pi h}{w_i \sqrt{\epsilon_r} \sqrt{(\omega_c / \omega)^2 - 1}} \omega_c \quad (18)$$

h is the thickness of the dielectric substrate, ω_c is the dielectric angular frequency of HMSIW, and ω is the central angular

frequency in the designed coupler band. The electrical length θ_i of the lossless HMSIW transmission line is given by

$$\theta_i = \gamma_i l_i \quad (19)$$

where the propagation constant γ_i can be calculated as

$$\gamma_i = \sqrt{\left(\frac{\pi}{2w_i}\right)^2 - \omega^2 \epsilon_r \mu_r} \quad (20)$$

Based on (10–14), the coupling coefficient C and isolation coefficient Is of the four-port coupling network in Fig. 6(a) can be obtained as

$$S_{31} = \frac{S_{11e} - S_{11o}}{2} \quad (21a)$$

$$S_{41} = \frac{S_{21e} - S_{21o}}{2} \quad (21b)$$

$$C = 20 \log |S_{31}| \quad (21c)$$

$$Is = 20 \log |S_{41}| \quad (21d)$$

After determining the partial sizes of the HMSIW transmission line, the coupling degree C required by design is brought into the above formulas to calculate the remaining transmission line size of the overall coupling structure without compensation ($B = 0$). Next, the equivalent capacitance B is controlled by adjusting the size of the compensation structure to optimize the reflection coefficient, in-band flatness, and directivity in the entire frequency band. It is worth noting that B can be determined by changing the length of $L_{s\text{mm}}$. Any reactance value can be achieved when the length of $L_{s\text{mm}}$ is within half the wavelength λ_g . W_s should be controlled within half of l_2 to avoid unnecessary coupling. Figure 7 shows the influence of changing the coupling branch width w_2 on the coupling degree after other dimensions of the coupling structure are determined. The coupling degree can be controlled by changing the value of w_2 to achieve the required coupling characteristics.

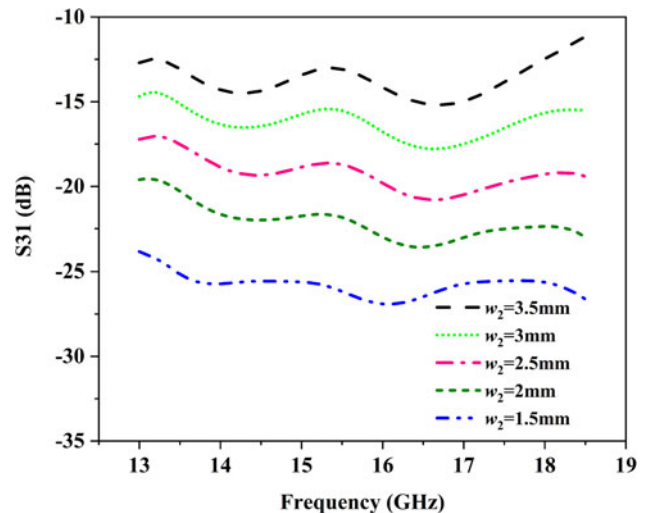


Fig. 7. Effect of the parameter w_2 on the coupling degree.

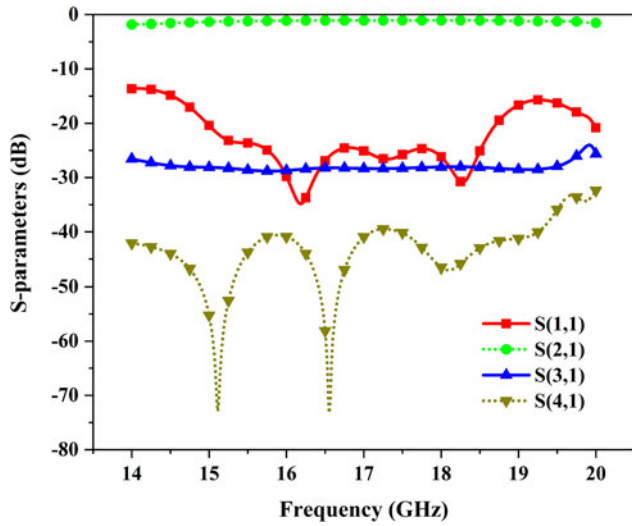


Fig. 8. Simulated S-parameters of the weak coupling coupler with compensation structure.

Based on the above explanation, the design and optimization procedures for the size of the weak coupling coupler are summarized as follows.

1) Selecting a suitable dielectric substrate according to the frequency band required by the design to obtain the dielectric constant ϵ_r . The values of W_H , p , and d are obtained by using the cut-off frequency f_{mn} of the SIW structure and the general SIW rules.

- 2) Selecting the appropriate length l_2 of the vertical metal wall. l_2 shall not exceed half of W_H .
- 3) Z_1 can be set freely. The equivalent width w_1 of the straight branch can be obtained by bringing the value of Z_1 into equation (18). The propagation constant γ_1 and equivalent length l_1 can be obtained by bringing w_1 into equations (19) and (20).
- 4) Taking the coupling degree C required by design and other calculated variables into equations (11–21), and calculating the equivalent width w_2 of coupling branch.
- 5) Optimizing $L_{s\text{mm}}$ and W_s in the electromagnetic simulation software, and adjusting the coupling and isolation in the entire frequency band. $L_{s\text{mm}}$ and W_s should be less than $\lambda_g/2$ and $l_2/2$, respectively.
- 6) Adjusting the width w_m and w_t of the SIW-microstrip transition to obtain good matching performance.

The weak coupling HMSIW couplers are simulated, and shown in Fig. 8. In 14.5–19.36 GHz, the return loss S_{11} exceeds 15 dB, the S_{31} and S_{21} are 28.3 ± 0.5 and -1 ± 0.3 dB, the directivity is greater than 12 dB, and the relative bandwidth is 28.5%. It can be concluded that both structures can realize broadband weak coupling performance and have excellent directivity and flatness.

Experimental results

To prove the HMSIW weak-coupling design theory described in the second part, a broadband weak coupling HMSIW coupler is fabricated and tested. The PCB layout and configuration are shown in Fig. 9.

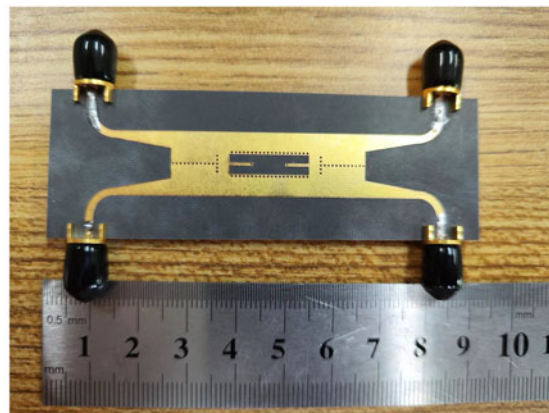
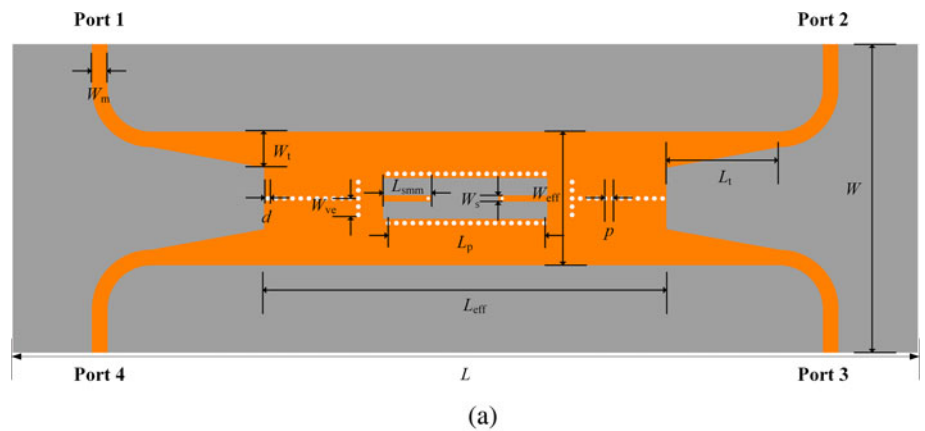
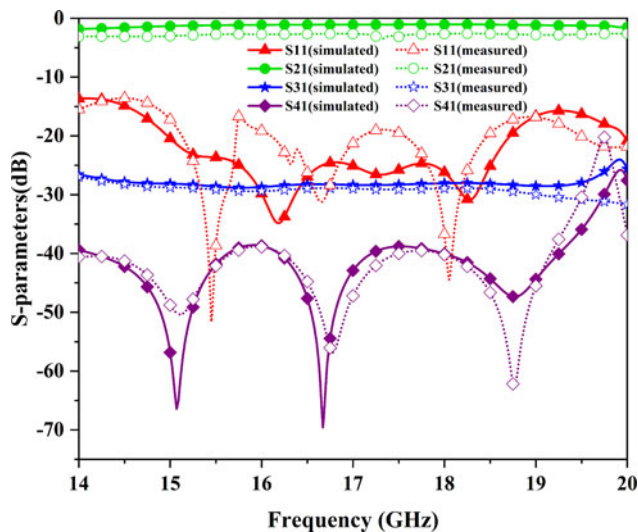


Fig. 9. (a)The configuration and (b) PCB layout of the HMSIW coupler.

(b)

Table 1. Dimensions of the coupler module (unit: mm)

Parameter	Value	Parameter	Value	Parameter	Value
W_m	1.5	W_t	3.5	W_{ve}	1.85
d	0.5	L_{smm}	4.85	W_s	0.6
W_{eff}	13	L_p	15	ρ	0.8
L_{eff}	39.1	L_t	11	W	40
L	88				

**Fig. 10.** Measured and simulated S-parameters of the proposed coupler.

The substrate is Rogers 5880 with copper thickness and PCB thickness are 0.035 and 0.508 mm, respectively. All metal vias are identical in size. The final physical design sizes of the coupler are shown in Table 1.

The four ports are connected with the SMA connectors, respectively. The large size of the dielectric laminate is conducive

to the convenience of testing. Therefore, the coupler is fabricated on a sizeable dielectric laminate. Figure 10 shows the measured and simulated S-parameters of the coupler manufactured this time. The coupler operates in 14.5–18.75 GHz, with S_{11} below -15 dB and isolation (S_{41}) down -39 dB. The transmission coefficient (S_{21}) and the coupling coefficient (S_{31}) are -2.5 ± 0.5 and -29 ± 0.5 dB, respectively, within 25.5% of the relative bandwidth range. The relative bandwidth of the measurement results is 3% lower than that of the simulation results. S_{21} includes the line loss caused by SMA connectors and test cables, and the actual insertion loss is -1.3 ± 0.4 dB. Considering the flexibility of the dielectric substrate, manufacturing and measurement errors, the simulation results are consistent with the measured results.

The comparison between the proposed weak coupling coupler and other couplers is shown in Table 2. It can be seen that the coupler has better directivity, and in-band flatness than other SIW weak coupling couplers in broadband. In addition, the weak coupling coupler designed in this paper has a smaller coupling coefficient than the published weak coupling SIW coupler. The performance will decline when these couplers achieve the same coupling. Currently, some proposed SIW coupler architectures [10–15, 18–20] can accomplish a weak coupling by changing parameters, but the performance will deteriorate seriously, and the directivity can hardly be used as an indicator to measure, which can also prove the superiority of the weak coupler proposed in this study.

Table 2. Comparison with other referenced coupler modules

Ref.	Coupler type	Bandwidth (GHz)/ (%) ^a	Coupling (dB)	Directivity (dB)	Return loss (dB)	Insertion loss (dB)	Size ($\lambda_g \times \lambda_g$)
[5]	SIW	35–42/18	10.5 ± 0.5	>8	<-12	>-3	2.34×2.34
[13]	SIW	36–42/15	25 ± 2.5	>6	<-18	>-3	2.8×1.9
[15]	SIW	24–38/45	17.5 ± 2.5	>3	–	>-2	2.3×1.1
[21]	PRGW	26–34/26.5	10 ± 0.5	>10	<-15	>-0.5	1.1×0.97
[22]	HMSIW	8.5–10.5/21	7.5 ± 1.6	>5.6	<-13.3	>-2	3.06×1.2
[23]	SIW	28–38/30	20 ± 1	>6	<-18	>-0.58	N.R
[24]	PRGW	28–32/13	3.6 ± 0.75	>10	<-15	>-3.5	1.1×1.1
This work	HMSIW	14.5–18.75/25.5	29 ± 0.5	>10	<-15	>-1.7	3.2×1.01

N.R, Not reported.

λ_g : The operating wavelength at the center frequency.

^aRelative bandwidth.

Conclusion

In this paper, a novel weak coupling broadband HMSIW coupler is proposed, simulated, and fabricated. The overall structure is similar to a branch-like coupler to achieve weak coupling characteristics. The compensation reactance is added to the parallel branches of the network to improve the bandwidth and directivity. The measurement and simulation are basically consistent. Under the operating frequency of 25.5% relative bandwidth, the coupling is 29 ± 0.5 dB, and the isolation is more significant than 39 dB. The coupler proposed in this paper complements the study of the SIW coupler in weak coupling mode. It has excellent broadband and directivity characteristics and can be applied to Ku-band power detection and power combiner circuit for satellite communication.

Acknowledgements. This work was supported by Zhejiang Provincial Public Technology Research Project (Grant LGG21F010006) and Project of Ministry of Science and Technology (Grant D20011).

Conflict of interest. None.

References

1. Wu KE, Bozzi M and Fonseca NJG (2021) Substrate integrated transmission lines: review and applications. *IEEE Journal of Microwaves* **1**, 345–363.
2. Chen JX, Hong W, Hao ZC, Li H and Wu K (2006) Development of a low cost microwave mixer using a broad-band substrate integrated waveguide (SIW) coupler. *IEEE Microwave and Wireless Components Letters* **16**, 84–86.
3. Hao ZC, Hong W, Chen JX, Zhou HX and Wu K (2006) Single-layer substrate integrated waveguide directional couplers. *IEEE Proceedings-Microwaves Antennas and Propagation* **153**, 426–431.
4. Pasian M, Bozzi M and Perregrini L (2014) Crosstalk in substrate integrated waveguides. *IEEE Transactions on Electromagnetic Compatibility* **57**, 80–86.
5. Shi X and Zhu X (2018) Design of cruciform directional coupler with capacitive slots based on SIW. In *2018 International Conference on Microwave and Millimeter Wave Technology (ICMMT)*, pp. 1–3.
6. Shen W, Yin WY and Sun XW (2011) Compact substrate integrated waveguide (SIW) filter with defected ground structure. *IEEE Microwave and Wireless Components Letters* **21**, 83–85.
7. Khan AA and Mandal MK (2016) Miniaturized substrate integrated waveguide (SIW) power dividers. *IEEE Microwave and Wireless Components Letters* **26**, 888–890.
8. Anand S and Rokhini D (2019) A double line SIW cavity backed antenna for WLAN applications. *International Journal of RF and Microwave Computer-Aided Engineering* **29**, e21861.
9. Wang Z and Park CW (2012) Novel substrate integrated waveguide (SIW)-based power amplifier using SIW-based filter to suppress up to the fourth harmonic. In *2012 Asia Pacific Microwave Conference Proceedings*, pp. 830–832.
10. Liu B, Hong W, Wang YQ, Lai QH and Wu K (2007) Half mode substrate integrated waveguide (HMSIW) 3-dB coupler. *IEEE Microwave and Wireless Components Letters* **17**, 22–24.
11. Liu Z, Xiao G and Mao J (2015) An approximate method to predict the characteristics of SIW-based directional coupler. In *2015 IEEE 4th Asia-Pacific Conference on Antennas and Propagation (APCAP)*, pp. 529–530.
12. Deng HW, Sun L, Zhu JM, Han YK and Xue YF (2020) High CM suppression balanced SIW BPF and HMSIW directional coupler utilising perfect electric conductor/perfect magnetic conductor characteristic. *IET Microwaves, Antennas & Propagation* **14**, 1061–1068.
13. Shi X and Zhu X (2017) Design of SIW parallel coupling coupler at q-band. In *2017 Sixth Asia-Pacific Conference on Antennas and Propagation (APCAP)*, pp. 1–3.
14. Liu Z and Xiao G (2016) Design of SIW-based multi-aperture couplers using ray tracing method. *IEEE Transactions on Components, Packaging and Manufacturing Technology* **7**, 106–113.
15. Wang X, Deslandes D, Feng W, Chen H and Che W (2020) Coupling analysis of adjacent substrate-integrated waveguides based on the equivalent transmission line model. *IEEE Transactions on Microwave Theory and Techniques* **68**, 1347–1354.
16. Bozzi M, Perregrini L and Wu K (2008) Modeling of radiation, conductor, and dielectric losses in SIW components by the BI-RME method. In *2008 European Microwave Integrated Circuit Conference*, pp. 230–233.
17. Iqbal A, Tiang JJ, Wong SK, Alibakhshikenari M, Falcone F and Limiti E (2020) Miniaturization trends in substrate integrated waveguide (SIW) filters: a review. *IEEE Access* **8**, 223287–223305.
18. Liu S and Xu F (2017) Minimized multi-layer substrate integrated waveguide 3-dB small aperture coupler. *Microwave and Optical Technology Letters* **59**, 3201–3205.
19. Liu S and Xu F (2018) Compact multilayer half mode substrate integrated waveguide 3-dB coupler. *IEEE Microwave and Wireless Components Letters* **28**, 564–566.
20. Wang X, Zhou D, Zhang D, Wang Y, Lv D and Zhang Y (2021) Balanced-to-unbalanced and balanced-to-balanced filtering rat-race couplers using multilayer substrate integrated waveguide cavities. *IET Microwaves, Antennas & Propagation* **15**, 1967–1981.
21. Ali MMM, Haraz OM, Afifi I, Sebak AR and Denidni TA (2022) Ultra-wideband compact millimeter-wave printed ridge gap waveguide directional couplers for 5G applications. *IEEE Access* **10**, 90706–90714.
22. Qiu LL, Zhu L, Ouyang ZA and Deng L (2021) Wideband butler matrix based on dual-layer HMSIW for enhanced miniaturization. *IEEE Microwave and Wireless Components Letters* **32**, 25–28.
23. Doghri A, Djerfati T, Ghiotto A and Wu K (2014) Substrate integrated waveguide directional couplers for compact three-dimensional integrated circuits. *IEEE Transactions on Microwave Theory and Techniques* **63**, 209–221.
24. Ali MMM, El-Gendy MS, Al-Hasan M, Mabrouk IB, Sebak A and Denidni TA (2021) A systematic design of a compact wideband hybrid directional coupler based on printed RGW technology. *IEEE Access* **9**, 56765–56772.



Minghui You was born in Gansu Province, China, in 1998. He received the BE degree in electronic and information engineering from Chengdu University of Technology, in 2020. He is pursuing the ME degree in the School of Electronic Information, Hangzhou Dianzi University, Hangzhou, China. His current research interests include Doherty power amplifier, substrate integrated waveguide, and load modulated balanced power amplifier.



Guohua Liu received the M.S. degree from the East China Normal University, Shanghai, China, in 2004, and the Ph.D. degree in electronic science and technology from the Hangzhou Dianzi University (HDU), Hangzhou, China, in 2020. He is currently a professor with HDU. His research interests include microwave circuits, sensors, antennas, and wireless systems design.



Zhiqun Cheng received the B.S. and M.S. degrees from the Hefei University of Technology, Hefei, China, in 1986 and 1995, respectively, and the Ph.D. degree in microelectronics and solid state electronics from the Shanghai Institute of Metallurgy, Chinese Academy of Sciences, Shanghai, China, in 2000. From 1986 to 1997, he was a teaching assistant and a lecturer with the Hefei University of Technology. He is currently a professor with Hangzhou Dianzi University. His research interests include microwave theory and technology, MMIC, power amplifier, and RF front end.